nature neuroscience

ARTICLES

https://doi.org/10.1038/s41593-019-0494-0

Widespread temporal coding of cognitive control in the human prefrontal cortex

Elliot H. Smith[1,9], Guillermo Horga[2,9], Mark J. Yates[3], Charles B. Mikell[4], Garrett P. Banks[3], Yagna J. Pathak[3], Catherine A. Schevon[5], Guy M. McKhann II[3], Benjamin Y. Hayden[6], Matthew M. Botvinick[7] and Sameer A. Sheth[8*]

When making decisions we often face the need to adjudicate between conflicting strategies or courses of action. Our ability to understand the neuronal processes underlying conflict processing is limited on the one hand by the spatiotemporal resolution of functional MRI and, on the other hand, by imperfect cross-species homologies in animal model systems. Here we examine the responses of single neurons and local field potentials in human neurosurgical patients in two prefrontal regions critical to controlled decision-making, the dorsal anterior cingulate cortex (dACC) and dorsolateral prefrontal cortex (dlPFC). While we observe typical modest conflict-related firing rate effects, we find a widespread effect of conflict on spike-phase coupling in the dACC and on driving spike-field coherence in the dlPFC. These results support the hypothesis that a cross-areal rhythmic neuronal coordination is intrinsic to cognitive control in response to conflict, and provide new evidence to support the hypothesis that conflict processing involves modulation of the dlPFC by the dACC.

As we navigate through our daily lives, we are often confronted with choices involving competing or conflicting potential courses of action[1]. To resolve this cognitive conflict, we must summon additional cognitive resources—that is, we must both monitor and resolve the conflict. For example, imagine driving through a busy city center area and seeing the next traffic light turn green—normally a signal to go—but a slow-moving pedestrian is on the pedestrian crossing. To make the optimal decision as to whether to brake or swerve, the driver must summon additional cognitive resources to assess the pedestrian's speed, estimate the trajectory of the car, and determine whether other cars are following closely behind. This capacity to monitor conflict and implement control is a vital, yet poorly understood, element of the repertoire of flexibly intelligent organisms[2,3]. Understanding its mechanisms is essential for developing treatments for neuropsychiatric disorders associated with impaired conflict processing, and, since conflict is a useful model for other types of executive control, of control in general[4].

Much research has implicated the dorsal prefrontal cortex, especially the dorsal anterior cingulate cortex (dACC) and dorsolateral prefrontal cortex (dlPFC), in the monitoring and resolution of cognitive conflict[5]. For example, a large amount of imaging and electrophysiology data from humans and non-human animals supports the hypothesis that these regions play a critical role in one or both processes[6–13]. Moreover, lesions to these regions lead to a variety of impairments in control functions[14]. Prominent computational and theoretical models ascribe to these regions several features that are critical to a control process: monitoring goal-relevant variables, evaluating relative costs and benefits of choice alternatives, maintaining rule sets and goal-related information in working memory, and producing adaptive biases towards more successful behavior[3,15–18]. This work dovetails with careful computational studies on how systems with limited cognitive capacity can trade off between multiple competing sources of guidance[18,19]. That work in turn results in specific circuit-level predictions about how cognitive control can be implemented in response to conflict. In particular, the study suggests that the dACC serves as a conflict monitor and that the dlPFC, located downstream of the dACC, serves to implement conflict-related changes[2,3,20]. The idea that these two regions are both involved in conflict processing but have distinct roles has been difficult to test given the paucity of studies that directly compare the activities of these two regions using neuron-level recording methods.

On the one hand, human neuroimaging studies find clear correlates of conflict but lack the temporal resolution to identify circuit-level correlates[21]. On the other hand, primate neurophysiology studies, which have high temporal and spatial resolution, have generally failed to find clear correlates of cognitive conflict[13,22]. Rodents do not have a clear homolog of either the dACC or dlPFC, making interpretation of data from rodent studies challenging[23,24]. The reasons for the disconnect between non-human primate electrode recording studies and human neuroimaging are not clear. One reason may be that animal studies require a very large number of trials; the resulting overtraining may systematically alter conflict processing[25,26]. Another likely factor is that functional magnetic resonance imaging (fMRI) and single unit activity (SUA) do not have clear one-to-one mapping, so there may be other features of brain responses that predict conflict other than average firing rate responses.

Control, like many other aspects of executive function, requires coordination of activity across regions. This has led to the hypothesis that the major signatures of control would be observed in relation to the local field potential (LFP), which is thought to provide a mechanism for coordination across multiple brain structures[27]. LFP is distinct from unit activity and seems to be a better predictor of

[1]Department of Neurosurgery, University of Utah, Salt Lake City, UT, USA. [2]New York State Psychiatric Institute, New York, NY, USA. [3]Department of Neurological Surgery, Columbia University Medical Center, New York, NY, USA. [4]Department of Neurosurgery, Stony Brook University, Stony Brook, NY, USA. [5]Department of Neurology, Columbia University Medical Center, New York, NY, USA. [6]Department of Neuroscience, University of Minnesota, Minneapolis, MN, USA. [7]DeepMind, London, UK. [8]Department of Neurosurgery, Baylor College of Medicine, Houston, TX, USA. [9]These authors contributed equally: Elliot H. Smith, Guillermo Horga. *e-mail: Sameer.Sheth@bcm.edu

hemodynamic responses than average unit firing in some cases[28,29]. Furthermore, an extensive electroencephalography (EEG) literature provides reason to believe that oscillations contain information critically related to conflict processing. For example, variations in theta-range (4–8 Hz) oscillations over frontal EEG contacts, known as frontal midline theta, have repeatedly been shown to reflect conflict and error processing, attentional control, and reinforcement-learning signals[30,31]. Such findings have been extended and refined with the few existing studies using human intracranial EEG[32,33]. This literature has led to an increasing number of theories positing a fundamental role for oscillatory activity in decision-making and cognition more generally[3,34]. An increasingly substantial body of evidence has demonstrated the importance of neuronal spiking activity as it relates to the background LFP. This alignment of spiking with LFPs, or spike-field coherence (SFC), is a potent channel for coordination of neuronal populations, both locally and across brain regions[35]. For these reasons, our analyses focused on the SFC within the dACC and dlPFC.

Here we examined simultaneously collected single-neuron responses and LFPs in the dACC and dlPFC in human neurosurgical patients. We found modest neuronal firing rate correlates of conflict in the dACC and negligible ones in the dlPFC. By contrast, we found robust effects of conflict on the preferred phase of spiking in the dACC (but not in the dlPFC), but greater conflict-related SFC changes in the dlPFC than in the dACC. These results support the hypothesis that processing cognitive conflict requires cross-areal coordination mediated, at least in part, by oscillatory activity. Moreover, they are consistent with the hypothesis that conflict processing involves monitoring by the dACC and control by the dlPFC[20]. Finally, our results show how neural codes that combine information in the spiking and oscillatory frequency (LFP) domains can facilitate the types of coordinated computation needed for executive control and provide important constraints on computational models of conflict processing.

Results

Limited, mixed firing rate code for conflict in the dACC. We simultaneously recorded firing rates of single neurons in the dACC, and LFPs in both the dACC and dlPFC, in six human patients with medically refractory epilepsy undergoing intracranial recordings to detect seizures (Fig. 1a and Supplementary Tables 1–3). Participants performed the multi-source interference task (MSIT), a task that independently manipulates both spatial (Simon) and flanker (Eriksen) types of decision conflict (Fig. 1b). Participants had an overall low error rate (average of 1.4 ± 2.7% per session) and exhibited the hallmark behavioral signature of tasks demanding cognitive control: increasing reaction time with increasing level of decision conflict (Fig. 1c).

We recorded firing rates from 136 well-isolated dACC neurons (Fig. 2a). To classify neurons on the basis of firing rate coding of task-relevant variables, we used a sliding-window generalized linear model (GLM) incorporating three factors corresponding to the three main task variables: decision conflict, response identity, and feedback valence. We defined decision conflict as the sum of the two binary variables corresponding to the two forms of conflict.

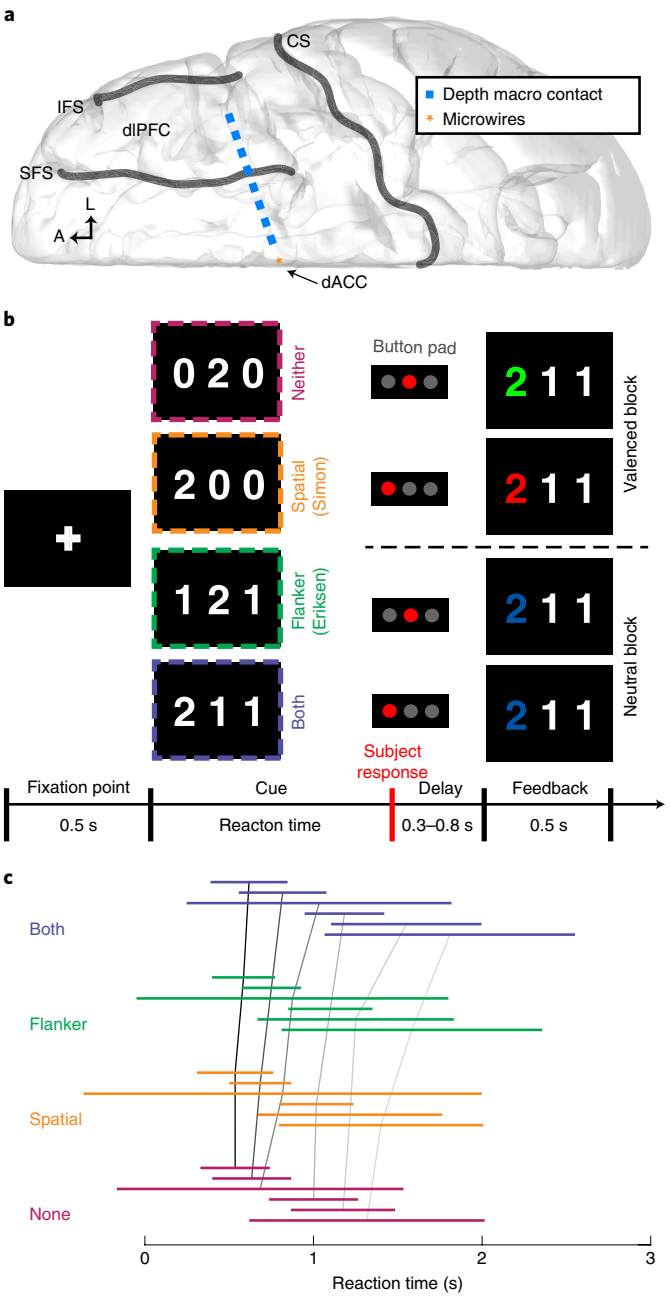

Fig. 1 | Recording configuration, task description, and behavioral performance. a, Diagram of the intracranial implant including a stereotactically placed intracerebral depth electrode with macroelectrodes (blue squares) along the shaft from the dlPFC to the dACC and microwire electrodes in the dACC. A, anterior; CS, central sulcus; IFS, inferior frontal sulcus; L, lateral; SFS, superior frontal sulcus. **b**, MSIT. The participant sees a cue consisting of three numbers and has to identify the unique number ('target') and respond with a button push: left button if the target is 1, middle if the target is 2, and right if the target is 3. Incongruence between the location of the target number in the three-digit sequence and location of the correct button in the three-button pad produces spatial (Simon) conflict. The distracting presence of numbers that are valid button choices (1, 2, or 3, versus 0, which is not a valid choice) produces flanker (Eriksen) conflict. Trials can also have neither type of conflict or both types. In all four example trials shown, 2 is the target; therefore, the middle button is the correct response. Following the response, valenced (green for correct, red for incorrect; two example trials are shown above the dashed line) or unvalenced (blue regardless of correctness, two example trials are shown below the dashed line) feedback is provided in alternating blocks of ten trials. **c**, Line plots of reaction time distributions across all patients. Each colored line represents 2 s.d. of reaction times centered on the mean reaction time and color-coded according to each conflict condition. Black and gray lines connect the means across conflict conditions within each patient. There was a statistically significant difference among conflict conditions (generalized linear mixed effects model, $t_{3881} = 2.36$, $P = 0.01$). Reaction time distributions for each participant and session are shown in Supplementary Fig. 7.

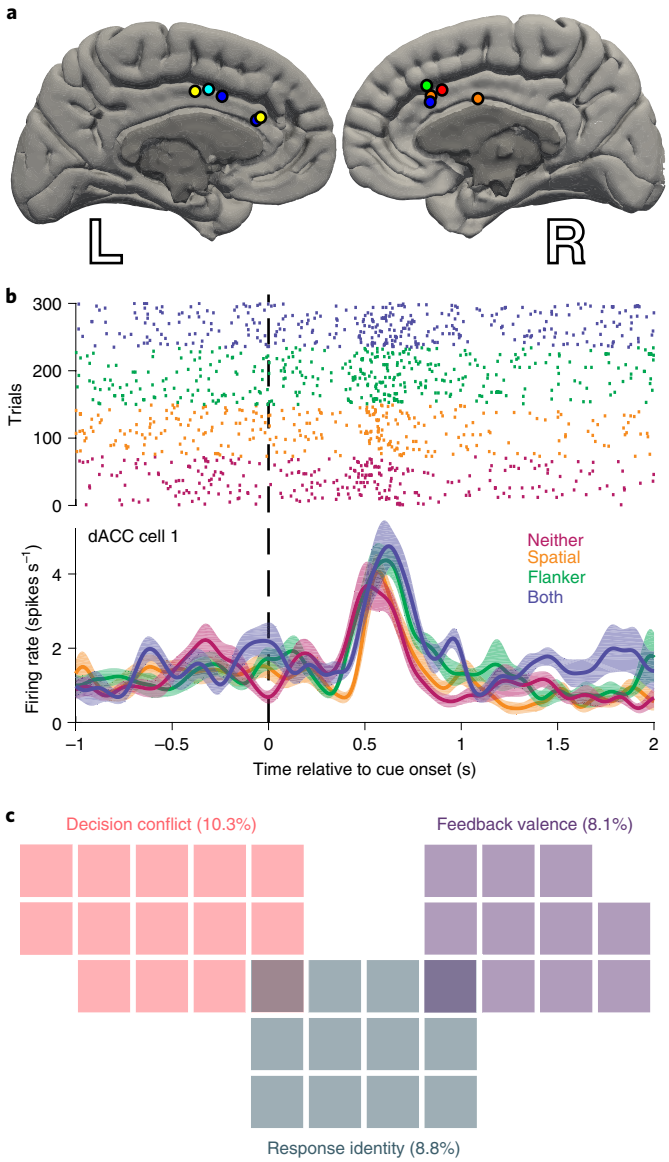

Fig. 2 | Rate coding of task-relevant variables in human dACC neurons. **a**, Microwire recording locations, with a different color for each participant. **b**, Example dACC raster plot and firing rate over conflict conditions for a representative neuron that shows rate coding for decision conflict. Shaded regions represent s.e. ($n = 72$ trials for no conflict, 77 trials for spatial conflict, 85 trials for flanker conflict, and 66 trials for both conditions). **c**, Venn diagram showing only the dACC neurons that were selective for specific task features, as determined by the sliding GLM. Each colored square represents one neuron, with the percentage of total ($n = 136$) neurons indicated in parentheses.

We focused our analysis on the period after cue presentation and before the behavioral response. We therefore chose a time window 250–750 ms after cue presentation for the subsequent analyses. In our sample, 10.3% of dACC neurons ($n = 14$ of 136) were selective for decision conflict (Fig. 2b), 8.8% ($n = 12$ of 136) were selective for response identity (Supplementary Fig. 1a), and 8.1% ($n = 11$ of 136) were selective for feedback valence (Supplementary Fig. 1b). There was very little overlap among the different neuron classes, suggesting that these forms of conflict are encoded in largely disjointed sets of cells (Fig. 2c). The majority of dACC neurons recorded (72.8%, $n = 99$ of 136) did not exhibit selectivity for any of the task variables based on firing rate. Nonetheless, it is clear that some human dACC neurons do use a detectable firing rate-coding scheme for task-relevant features, although these neurons are fairly uncommon.

Temporal code for decision conflict in the dACC. We next tested the hypothesis that PFC neurons use a temporal-coding strategy in the context of controlled decision-making. Of the three main task features, we focused our analysis on decision conflict, as this was the primary task manipulation (analyses of other features are presented in Supplementary Fig. 2). Specifically, we hypothesized that temporal patterns of neuronal spiking relate to population oscillatory activity, and that this relationship is modulated in a conflict level-dependent manner.

We measured the SFC for each neuron in relation to the LFP in the dACC. We observed significant increases in the SFC in the beta and theta ranges. These findings indicate that dACC spike timing could be predicted from population-level oscillations in these two frequency ranges (henceforth we refer to neurons exhibiting this property as beta- and theta-coherent, respectively, Fig. 3). Beta-coherent neurons ($n = 50$, 36.8%) showed significant increases in coherence in the frequency range between 16.1 and 24.4 Hz (SFC permutation test, $P < 0.05$). Theta-coherent neurons ($n = 43$, 31.6%) showed cue-evoked changes in coherence between 2.9 and 9.2 Hz (SFC permutation test, $P < 0.05$). The observed SFC results were not driven simply by variations in LFP power (Supplementary Fig. 3).

Moreover, we observed a prominent phase code for decision conflict in these temporally coherent neurons. We measured the mean phase at which neurons fired in relation to the population LFP for neurons with a significance cluster that overlapped with the time window used to assess firing rate selectivity. We found a clear pattern of dependence on the amount of decision conflict in both theta- and beta-coherent neurons (Fig. 3c,g). Neurons generally fired before the LFP trough during high-conflict trials (that is, theta-coherent neurons fired before the theta trough and beta-coherent neurons fired before the beta trough) and after the LFP trough during low-conflict trials (Fig. 3d,h). The number of neurons that showed a phase-specific temporal code for decision conflict was larger than the number that showed a conventional rate code (McNemar's Test, $P < 10^{-3}$, $\chi^2 = 13.5$, Fig. 3i). Furthermore, the phase code and rate code were largely independent from each other: rate-coding neurons seldom showed a phase code, and vice versa (correlation between firing rate code and theta temporal code: $\rho = 0.03$, $P = 0.76$; correlation between firing rate code and beta temporal code $\rho = -0.02$, $P = 0.74$; Fig. 3j,k). These results show robust and widespread temporal coding of decision conflict in the dACC, particularly evident as a phase code, and independent of a co-existing and less prevalent rate code.

Relationship between dACC spiking activity and broader network LFP activity. We next addressed the question of how these largely distinct neuronal populations with different information-encoding strategies differentially participate in the implementation of controlled decisions. To do so, we examined their interactions with the broader network that has previously been implicated in cognitive control, which includes the dorsolateral prefrontal cortex (dlPFC). We examined the spike-triggered LFP (stLFP) of dACC neurons to determine the relationship between dACC spiking activity and the local dACC LFP as well as the distant dlPFC LFP (for example, Fig. 1a, recording locations for each patient are shown in Supplementary Fig. 4).

The average stLFP of dACC spikes with dACC LFP (dACC–dACC stLFP) showed a consistent deflection starting immediately after the spike and becoming maximally negative around 100 ms post-spike (Fig. 4, all neuron categories shown in Supplementary Fig. 5). The stLFP amplitude for the rate-coding neurons was significantly greater than that for the beta- or theta-coherent neurons,

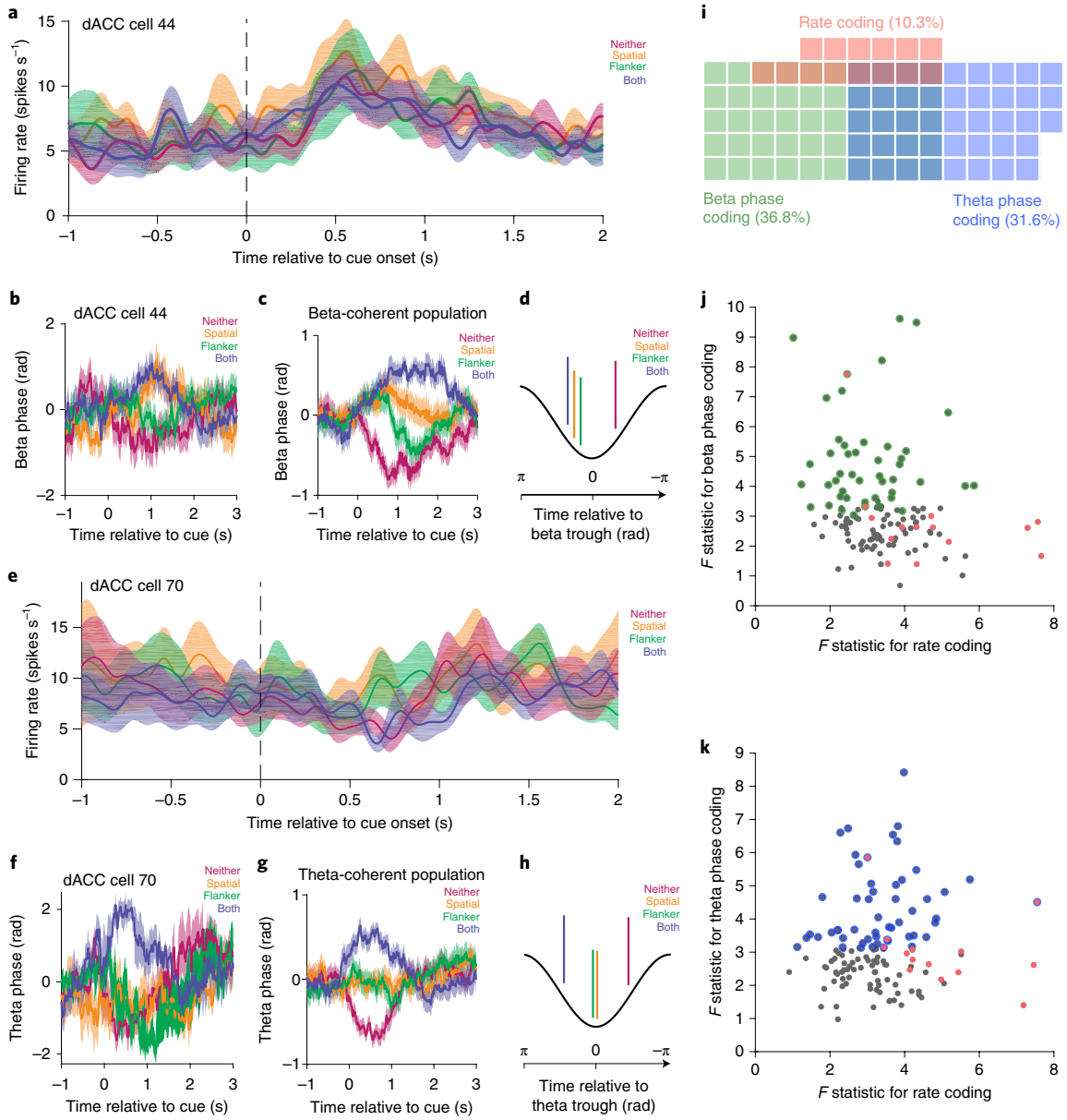

Fig. 3 | Robust phase coding in dACC neurons. a, Example dACC neuron with a firing rate that does not vary by conflict level (no firing rate code). **b**, Mean phase of SFC for a single beta-coherent neuron for each conflict condition. Shaded regions in **a** and **b** represent s.e. ($n = 72$ trials for no conflict, 77 trials for spatial conflict, 85 trials for flanker conflict, and 66 trials for both conditions). **c**, Mean phase of SFC across all beta-coherent neurons color-coded by conflict condition (LMM t-test, $t_{510} = 3.6$, $P = 4 \times 10^{-4}$). Shading represents s.e. across 50 beta-coherent neurons. **d**, Schematic showing mean spike phase for each conflict condition in beta-coherent neurons. **e**,**f**, Example dACC neuron that shows no firing rate code, but shows increased theta coherence, and mean phase of SFC for a single theta-coherent neuron for each condition ($n = 69$ trials for each conflict condition, shaded regions represent s.e.). **g**,**h**, Mean phase of SFC across all theta-coherent neurons color-coded by conflict condition (LMM t-test, $t_{510} = 3.1$, $P = 2 \times 10^{-3}$) and schematic showing mean spike phase for each conflict condition in theta-coherent neurons. Shading represents s.e. across 43 theta-coherent neurons. **i**, Venn diagram showing only the proportions of neurons that were beta phase-coding, theta phase-coding or rate-coding neurons for decision conflict. The proportion of beta or theta phase-coding neurons was significantly greater than that of rate-coding neurons (73 versus 14 neurons, McNemar's test, $\chi^2 = 13.5$, $P < 10^{-3}$). **j**,**k**, For each neuron, the maximum F statistic from the beta (**j**) or theta (**k**) phase code F statistics plotted against the maximum F statistic from the firing rate GLM (Spearman's ρ for theta: $\rho = 0.03$, $P = 0.76$; for beta: $\rho = -0.08$, $P = 0.32$; two-sided t-tests). Scatter plots show statistics for all 136 neurons. Significant rate-coding cells are shown in pink, and significant phase-coding cells are indicated with colored circles for each frequency range, as in **i**.

which in turn was significantly greater than that for the non-coding neurons and null distribution (Fig. 4a–c).

Spiking activity in the dACC also interacted with LFP in the dlPFC. SFC analysis between dACC spikes and dlPFC LFPs again revealed prominent temporal coding, with both beta- and theta-coding neuronal populations (Supplementary Fig. 6). dACC spikes were also associated with significant deflections in dlPFC LFP (dACC–dlPFC stLFP) (Fig. 4d,e). These stLFPs followed a similar pattern to the dACC–dACC stLFPs, with the greatest stLFP in rate-coding neurons, a lesser but still significant stLFP in beta and theta phase-coding neurons, and non-significant stLFPs in non-coding neurons (Fig. 4f). More dACC units were coherent with dlPFC theta (49 units, 36.0%, mean significant frequency range 2.9–10.2 Hz, permutation tests $P < 0.05$), than they were with dlPFC beta (43 units, 31.6 %,

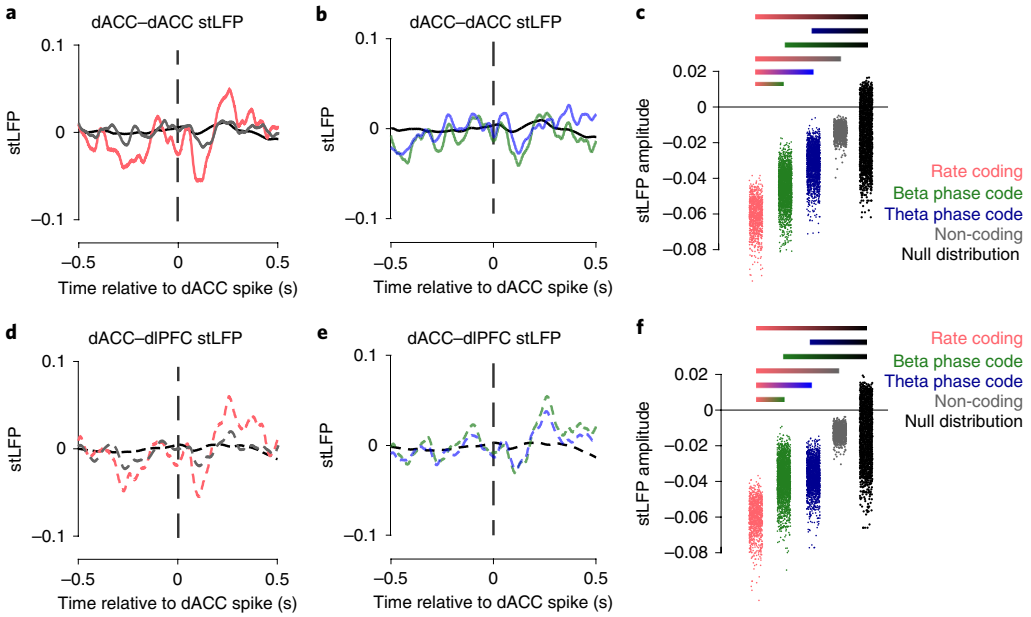

Fig. 4 | dACC neuronal interactions within a broader control network. a, stLFP waveforms evoked by dACC neurons on dACC LFP (dACC–dACC) for conflict-selective rate-coding neurons (pink, $n = 2{,}370$ spikes), non-coding neurons (gray, $n = 10{,}292$ spikes), and null distribution (black). **b**, dACC–dACC stLFP waveforms for temporal-coding neurons: beta-coherent (green, $n = 8{,}398$ spikes), theta-coherent (blue, $n = 7{,}581$ spikes), and null distribution (black). **c**, Distributions of dACC–dACC stLFP amplitudes for each neuron group in **a** and **b**. stLFP amplitudes were decorrelated by their covariance matrices and *z*-scored. **d**–**f**, stLFP waveforms evoked by dACC neurons on dlPFC LFP (dACC–dlPFC), dACC–dlPFC waveforms for temporal-coding neurons, and distributions for dACC–dlPFC stLFP amplitudes for each neuron group shown in **a**. Gradient bars in **c** and **f** show significant pairwise post-hoc comparisons of fixed effects (following omnibus LMM *t*-test, $t_{20,576} < 2.2$, $P < 0.02$; post hoc two-sided *t*-tests, all *P* values < 0.05).

mean significant frequency range for beta 18.1–25.9 Hz, permutation tests $P < 0.05$). The dACC–dlPFC phase code arose slightly later in beta-coherent neurons (Supplementary Fig. 6a,b, significant time range 0.8–2.4 s post-stimulus) and slightly earlier in theta-coherent neurons (Supplementary Fig. 6c,d, significant time range 0.1–2.5 s post-stimulus). The effect sizes for the dACC neurons that were coherent with dlPFC LFPs are shown in Supplementary Fig. 6e,f. The subpopulations of dACC neurons that cohered with beta- and theta-range LFPs in the dlPFC were mostly distinct from those that cohered with the dACC, yet their proportions did not differ significantly (Supplementary Fig. 6g, McNemar's Test, $P = 0.86$, $\chi^2 = 0.03$). These results indicate that spiking activity in a relatively small group of dACC neurons (that is, rate-coding neurons) correlates with increased post-synaptic activity in a broader prefrontal network encompassing the dACC and dlPFC.

Rate and temporal coding of task-relevant variables in the dlPFC. To determine whether the previous findings were unique to the dACC, we next tested for the presence of similar temporal-coding schemes in the dlPFC. We recorded single units and LFP from the dlPFC in a second cohort of nine neurosurgical patients: eight patients undergoing deep brain stimulation (DBS) surgery with microelectrode recordings and a subdural electrocorticography (ECoG) strip using a standard entry point over the dlPFC and one undergoing epilepsy monitoring with prefrontal subdural grid and strip electrodes and a Utah microelectrode array (UMA) in the dlPFC (Fig. 5a). Behavioral performance on the MSIT was similar in this cohort to that in the first cohort (Supplementary Fig. 7).

We recorded a total of 367 single units from the dlPFC in these nine individuals (Fig. 5). We analyzed the same time period (250–750 ms after cue presentation) as in the dACC analysis above. Using the same sliding GLM approach to test for firing rate selectivity, we found that a small proportion of neurons encoded conflict ($n = 15$, 4.1%). This proportion was not significantly greater than chance (exact test; $P > 0.05$) and, not surprisingly, was significantly smaller than the proportion found in the dACC (χ^2 test, $\chi^2 = 8.2$, $P = 4.3 \times 10^{-3}$). Additionally, 18 neurons were selective for response identity (4.9%, Supplementary Fig. 8a) and 24 were selective for feedback valence (6.5 %, Supplementary Fig. 8b, Fig. 5b).

SFC analysis revealed prominent theta-range SFC in the majority of recorded neurons ($n = 238$, 64.9%). The strength of coherence between spike timing and theta oscillations increased with higher levels of conflict (Fig. 5d–f). This effect was prominent enough to be visible across the entire population of recorded neurons (Fig. 5g) and was significant at the individual neuron level in the majority of cells ($n = 191$, 52.0%). Furthermore, we observed this pattern in neurons from each of the nine participants (mean ± standard deviation = 67.3% ± 19.9% of neurons from each participant). In contrast to its prominence in the dlPFC, only a small number of dACC neurons exhibited similar conflict-modulated scaling in SFC amplitude (Fisher's exact test, $P < 10^{-5}$). By contrast, the prominent phase-coding motif evident in the dACC was not apparent in the dlPFC. We found a slight precession of the SFC phase in all conditions, with similar error across conditions, yet no significant differences among phases for each condition. This means that the mean phase does not differ among conflict conditions, although the amplitude of SFC increases (Supplementary Fig. 9c). Thus, we observed a similar general theme of uncommon rate-coding but robust temporal coding in the dlPFC, but the specific temporal-coding schemes differed between dACC and dlPFC neurons. The overall thematic similarities demonstrate that the temporal-coding archetype is not unique to the dACC and suggest that temporal coding may be a conserved strategy across the PFC. This finding also underscores the value of asking not only whether certain types of information (for example, conflict[9]) are encoded in different PFC regions, but also how they are encoded.

Trial-to-trial variation in temporal coding and its relationship to behavior. Neural information processing should be stable against

noise yet flexible enough to meet unforeseen changes in cognitive demands, whether driven by external conditions or by internal fluctuations in arousal, attention, or goals[36]. Because these demands vary on a moment-to-moment basis, their trial-to-trial encoding should be detectable. We reasoned that a temporal-coding scheme, distributed over a population of neurons, may be able to effectively support such an on-demand, within-trial implementation of controlled responses.

Using sessions with more than 100 simultaneously recorded neurons, we considered whether a distributed population of neurons can encode a particular instance of conflict as a coherent population. We examined SFC among all simultaneously recorded dlPFC neurons during each trial and again found significant spike-theta coherence that increased in trials with higher levels of conflict (Fig. 6a). Measuring SFC at the single-trial level also afforded the opportunity to examine whether trial-to-trial variation in SFC can account for trial-to-trial variation in behavior. This analysis revealed that the duration of theta coherence predicted reaction time in each trial (linear mixed model (LMM), $t_{886}=2.9$, $P=0.002$). Furthermore, higher mean theta coherence across neurons during a given trial strongly predicted shorter reaction times in that trial, even after controlling for conflict level in the current trial, in the previous trial, and their interaction (Fig. 6b, theta coherence: $t_{883}=-4.22$, $P=2\times10^{-5}$). To control for any differences between LFP recorded from surface ECoG, and intraparenchymally recorded LFP, we examined within-trial SFC using down-sampled and filtered LFP across the UMA between 1 and 50 Hz. Similar within-trial SFC effects were observed using intraparenchymally recorded LFP (Fig. 6c, LMM, $t_{769}=-3.9$, $P=9.5\times10^{-5}$). Despite their well-established relationship to reaction time, all other effects in the model (current and previous trial conflict level and their interaction) were substantially weaker than the theta-coherence effect on reaction time ($t_{883}\leq|1.99|$, $0.065>P>0.045$). Higher mean coherence was unrelated to conflict level in the previous trial ($P=0.24$), also supporting the idea that the relationship between mean theta coherence and reaction times was not driven by behavioral adaptations due to previous-trial effects[37]. These results show that a temporal code distributed across a population of dlFPC neurons closely tracks moment-to-moment fluctuations in performance, including and beyond those imposed by the task, potentially supporting a mechanism that permits flexible adjustments to cognitive demands.

Discussion

We examined the responses of single neurons and LFP in two brain regions, the dACC and dlPFC, in human neurosurgical patients performing a conflict task. We found a small but significant population of neurons in the dACC (but not the dlPFC) with changes in firing rate that encode task conflict. Our previous report demonstrated conflict encoding at the level of a population of human dACC neurons[38], but our current observation of explicit conflict

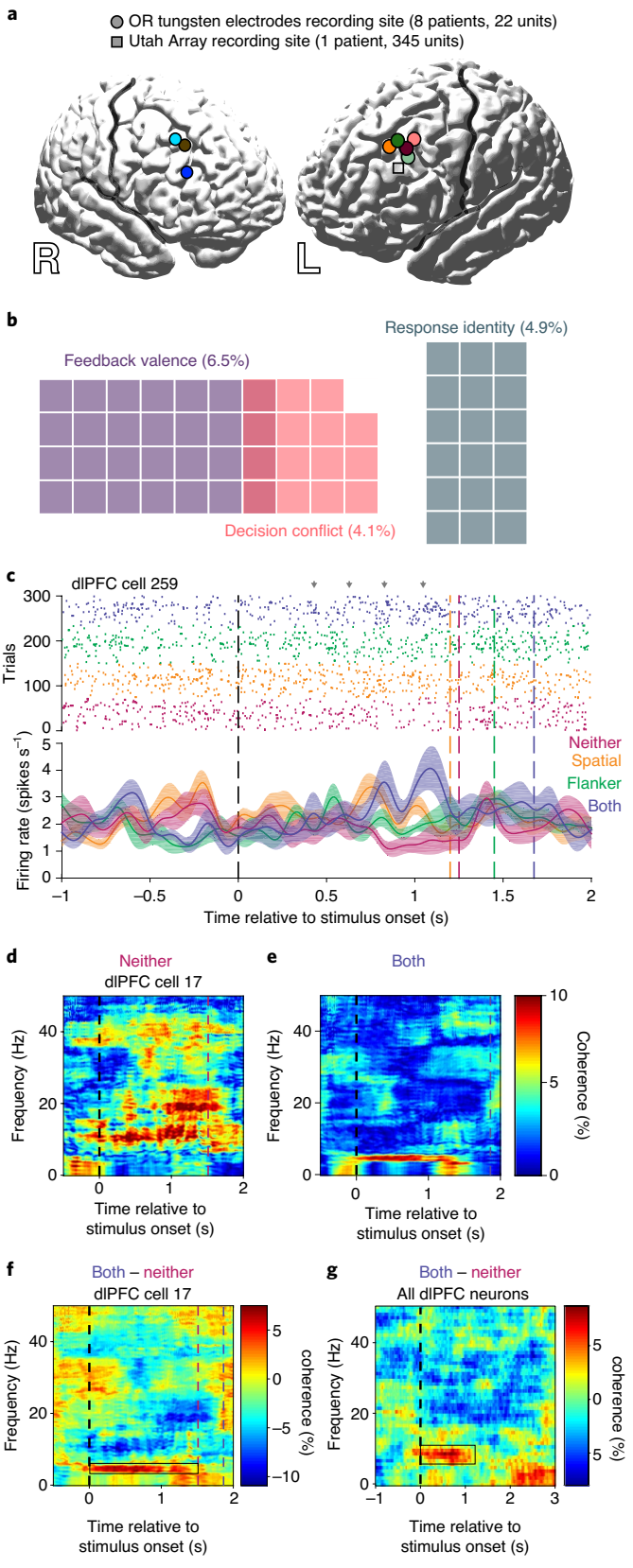

Fig. 5 | Temporal coding in human dlPFC neurons. a, Recording locations in the nine individuals from which dlPFC units were recorded. The circles represent patients with DBS and the square represents the patient with epilepsy. **b**, Venn diagram showing numbers (and percent, total $n=367$) of only the neurons that were selective for specific task features using a rate code. **c**, A representative dlPFC neuron with firing rate-coding and temporal (theta) coding (two-sided SFC permutation test, $P<0.05$) for decision conflict. Gray arrows highlight clusters of single unit spikes in a theta-coherent pattern. Shaded regions indicate s.e. ($n=58$ trials for no conflict, 86 trials for spatial conflict, 88 for flanker conflict, and 68 trials for both conditions). **d**,**e**, Representative coherograms for another dlPFC neuron averaged over no-conflict trials (**d**) and both-conflict trials (**e**). **f**, Difference coherogram between **d** and **e** illustrating increased coherence between spike timing and theta oscillations (boxed region) in higher-conflict trials. **g**, Mean difference coherogram averaged across all 367 dlPFC neurons recorded in all nine participants (boxed region shows significant clusters −0.1 to 1.2 s and 4.8 to 10.7 Hz, two-sided SFC permutation tests, all $P<0.05$). A total of 191 (52.0%) neurons demonstrated spike-theta coupling that scaled with conflict level (LMM t-test, $t_{886}=4.2$, $P=3\times10^{-5}$).

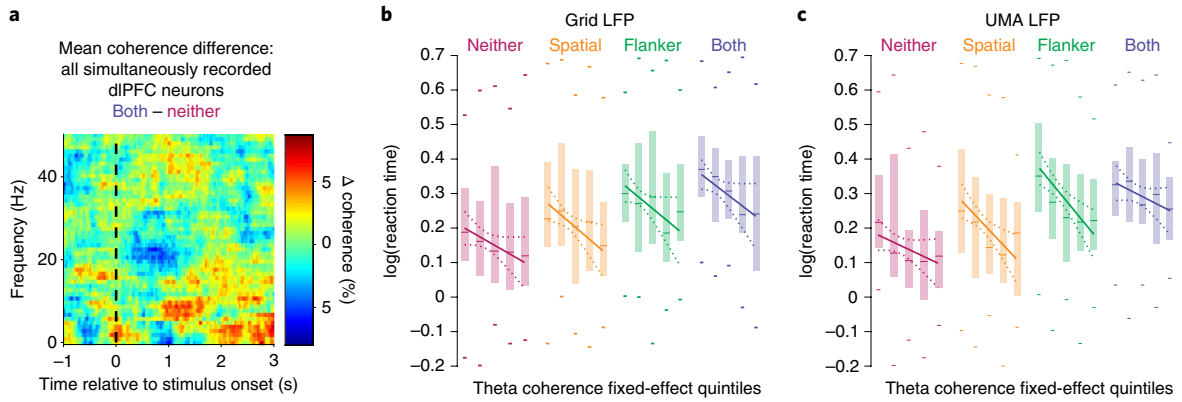

Fig. 6 | Trial-to-trial encoding of conflict via population theta coherence. a, Mean difference coherogram averaged across trials (sample sizes listed below) with more than 100 simultaneously recorded neurons on the dlPFC UMA, illustrating a significant difference in coherence across conflict conditions (the cluster of significant coherence was from 0.8 to 1.9 s and 5.4 to 10.7 Hz, two-sided SFC permutation test, all P values < 0.05). **b**, Box plots (box height, interquartile range; ticks, most extreme points; lines, medians) of theta coherence fixed-effect quintiles from the LMM versus log(reaction time) with overlaid regression lines for each conflict condition (n = 215 trials for no conflict, 222 trials for spatial conflict, 240 trials for flanker conflict, and 211 trials for both conditions). **c**, Box plots of theta coherence using down-sampled and filtered data from the UMA for coherence calculations (n = 187 trials for no conflict, 198 trials for spatial conflict, 208 trials for flanker conflict, and 176 trials for both conditions).

encoding at the level of individual neurons has not previously been reported in humans. Our new finding is important because it is inconsistent with the idea that ostensible conflict signals in mass action measures (such as BOLD) are an epiphenomenon[13]. The firing rate encoding of conflict in these neurons was most apparent before the decision occurred, suggesting that it may reflect conflict monitoring in the service of on-line control, rather than learning or trial-to-trial adjustment. More prominently, we found more widespread population encoding of conflict in the form of modulation of spike timing relative to ongoing LFPs. That is, a robust temporal code for decision conflict complements the more limited rate code. This temporal code seems to be independent of the spike code. Specifically, we observed this temporal code in neurons that did not exhibit a significant firing rate code, and the magnitudes of the two codes were independent across neurons.

An emerging concept bridging these perspectives is that the relationship between neuronal spiking and ensemble oscillatory activity is a critical feature that the brain uses to encode complex functional representations. Perhaps the most celebrated example of spike-oscillation synchrony is the theta phase precession observed in rat hippocampal and entorhinal place cells[39,40]. Similar temporal codes underlie the encoding of complex visual stimuli in the primary visual cortex[41], acoustic stimuli in the auditory cortex[36], and coordination of gaze and reaching movements in the parietal cortex[42]. It seems that there are similar neural representations of cognitive variables and spatial maps in the human ACC and mesial temporal lobe[43], respectively, and that both are linked to theta rhythmicity and phase coding[44]. Recent theoretical work has proposed a dynamical control mechanism for phase coding, thus providing explanatory power and opportunities for testing specific hypotheses[45]. These factors, together with the wide-ranging interconnected nature of the medial PFC, suggest that temporal coding in the medial PFC could both be a prominent coding scheme, and support a dynamical, distributed mechanism to influence a diverse array of brain areas[46].

Some previous work suggests that the dACC may integrate control-related variables into a general control signal and that the dlPFC may implement their effects; that is, the dACC may be a monitor and the dlPFC may be a controller[2,37]. Our results are broadly consistent with that proposed division of labor. First, in contrast to the dACC, we found a minimal effect of conflict on firing rate changes in dlPFC neurons, as if the dlPFC does not need to signal conflict per se. We did find a strong oscillatory code for conflict in the dlPFC, although it differed qualitatively from the one observed in the dACC: it was an increase in SFC without a concurrent alignment to phase such as that observed in the dACC. Oscillatory dynamic processes expand the coding space to allow optimized information formatting and consequently facilitate the sparsening of downstream representations, while simultaneously conferring stability of representations in the presence of noise[36]. From this perspective, a natural interpretation is that the dACC plays an upstream function, closer to the input (that is, the source of conflict), such as a detection or signaling role. Indeed, theoretical work suggests that impulses occurring at earlier phases of the cycle exert more control on the system[45]. That this phase relationship was not apparent in the dlPFC is consistent with the idea that it is functionally downstream of the dACC. In the same vein, theta-SFC coding in the dlPFC suggests its involvement in the downstream implementation of controlled behavior, particularly given that theta coherence is strongly correlated with faster responses even after controlling for external, task-derived demands, such as the amount of conflict in the current or previous trial cue. This finding accords with the idea that spike-theta coherence in the dlPFC may be a 'lingua franca' to support the implementation of controlled decision-making strategies, adjusting to the presence of sources of interference regardless of whether they are external (for example, the task or environment) or internal (for example, spontaneous attentional fluctuations)[30,31].

A substantial amount of research examining the neural bases of conflict detection and resolution has been conducted in non-human animals. Classically, much of this work reported no such correlates and suggested that ostensible conflict coding may be an epiphenomenon[13,47]. By contrast, at least two recent studies suggest that frank encoding of conflict may be observed in single neurons in non-human animals[48]. How can these results be reconciled? Our work suggests that two factors may be at play. First, the conflict coding observed in the dACC is greatest in the temporal, phase-locked domain and is much weaker in the rate domain, meaning that it may have been difficult to detect in some studies. Indeed, the hemodynamic correlates of conflict may be more strongly linked to the oscillatory patterns we observed than to the more modest rate code. Second, the weakness of the signal in animals may be compounded by the need for overtraining, which makes controlled behavior more automatized and may reduce the size of any neural signals. This effect would explain why firing rate effects seem to be larger in humans than in animals[38]. If so, this example illustrates one of the

major benefits of human intracranial recordings: that they allow for studies of rapidly and flexibly learned behaviors[25].

Predictions from this proposed functional specialization model can be tested with future work, including simultaneous recordings of larger neuronal populations in the dACC to measure the temporal structure of population representations, or closed-loop, single-pulse electrical stimulation at particular LFP phases to dynamically modulate cognitive control. Finally, this idea of functional specialization is not meant to imply a strict functional segregation between the dACC and dlPFC. The overall use of sparse rate-coding and widespread temporal-coding schemes highlights the need for an integrated understanding of the role of various neural coding strategies across prefrontal networks[46].

Conclusion: the soloists and the choir. Perhaps the most intriguing finding in our study is that the conflict rate-coding neurons, despite their low numbers, were associated with a disproportionately large relationship with LFP throughout the prefrontal network. We propose that this rate-coding minority may serve a specialized function of being particularly sensitive in detecting and signaling changes in conflict or, possibly, in demand for control. In other words, conflict-sensitive neurons may function as specialized 'soloists' in the medial PFC[49]. These soloists may serve as an early signal for the need to establish control, and then catalyze more widespread oscillatory activity throughout the network[46]. The larger population of temporal-coding neurons may then act as a 'choir' that stabilizes and amplifies the representation of task-relevant information. If this speculation is correct, then the soloist neurons may serve a local, intra-areal purpose, and the resulting oscillatory activity may serve to coordinate cross-regional coherent responses. This second form of responding would presumably be more robust to noise and more sensitive to regulation by top-down factors. This multi-faceted approach to representing relevant information may facilitate its efficient use and communication across neuronal systems.

Online content

Any methods, additional references, Nature Research reporting summaries, source data, statements of code and data availability and associated accession codes are available at https://doi.org/10.1038/s41593-019-0494-0.

Received: 24 May 2019; Accepted: 9 August 2019;
Published online: 30 September 2019

References

1. Botvinick, M. & Braver, T. Motivation and cognitive control: from behavior to neural mechanism. *Annu. Rev. Psychol.* **66**, 83–113 (2015).
2. Shenhav, A. et al. Toward a rational and mechanistic account of mental effort. *Annu. Rev. Neurosci.* **40**, 99–124 (2017).
3. Miller, E. K. & Cohen, J. D. An integrative theory of prefrontal cortex function. *Annu. Rev. Neurosci.* **24**, 167–202 (2001).
4. Abi-Dargham, A. & Horga, G. The search for imaging biomarkers in psychiatric disorders. *Nat. Med.* **22**, 1248–1255 (2016).
5. Cole, M. W., Repovš, G. & Anticevic, A. The frontoparietal control system: a central role in mental health. *Neuroscientist* **20**, 652–664 (2014).
6. Horga, G. et al. Adaptation to conflict via context-driven anticipatory signals in the dorsomedial prefrontal cortex. *J. Neurosci.* **31**, 16208–16216 (2011).
7. Blanchard, T. C., Strait, C. E. & Hayden, B. Y. Ramping ensemble activity in dorsal anterior cingulate neurons during persistent commitment to a decision. *J. Neurophysiol.* **114**, 2439–2449 (2015).
8. Botvinick, M., Nystrom, L. E., Fissell, K., Carter, C. S. & Cohen, J. D. Conflict monitoring versus selection-for-action in anterior cingulate cortex. *Nature* **402**, 179–181 (1999).
9. Carter, C. S. et al. Anterior cingulate cortex, error detection, and the online monitoring of performance. *Science* **280**, 747 (1998).
10. Kennerley, S. W., Behrens, T. E. J. & Wallis, J. D. Double dissociation of value computations in orbitofrontal and anterior cingulate neurons. *Nat. Neurosci.* **14**, 1581 (2011).
11. Hayden, B. Y., Heilbronner, S. R., Pearson, J. M. & Platt, M. L. Surprise signals in anterior cingulate cortex: neuronal encoding of unsigned reward prediction errors driving adjustment in behavior. *J. Neurosci.* **31**, 4178–4187 (2011).
12. Amemori, K. & Graybiel, A. M. Localized microstimulation of primate pregenual cingulate cortex induces negative decision-making. *Nat. Neurosci.* **15**, 776 (2012).
13. Nakamura, K., Roesch, M. R. & Olson, C. R. Neuronal activity in macaque SEF and ACC during performance of tasks involving conflict. *J. Neurophysiol.* **93**, 884 (2005).
14. Glascher, J. et al. Lesion mapping of cognitive control and value-based decision making in the prefrontal cortex. *Proc. Natl Acad. Sci. USA* **109**, 14681–14686 (2012).
15. Alexander, W. H. & Brown, J. W. Medial prefrontal cortex as an action-outcome predictor. *Nat. Neurosci.* **14**, 1338 (2011).
16. Shenhav, A., Straccia, M. A., Cohen, J. D. & Botvinick, M. M. Anterior cingulate engagement in a foraging context reflects choice difficulty, not foraging value. *Nat. Neurosci.* **17**, 1249 (2014).
17. Kolling, N. et al. Value, search, persistence and model updating in anterior cingulate cortex. *Nat. Neurosci.* **19**, 1280 (2016).
18. Collins, A. G. E. & Frank, M. J. Cognitive control over learning: creating, clustering, and generalizing task-set structure. *Psychol. Rev.* **120**, 190–229 (2013).
19. Gratton, G., Coles, M. G. & Donchin, E. Optimizing the use of information: strategic control of activation of responses. *J. Exp. Psychol. Gen.* **121**, 480 (1992).
20. MacDonald, A. W. Dissociating the role of the dorsolateral prefrontal and anterior cingulate cortex in cognitive control. *Science* **288**, 1835–1838 (2000).
21. Ebitz, R. B. & Hayden, B. Y. Dorsal anterior cingulate: a Rorschach test for cognitive neuroscience. *Nat. Neurosci.* **19**, 1278 (2016).
22. Blanchard, T. C. & Hayden, B. Y. Neurons in dorsal anterior cingulate cortex signal postdecisional variables in a foraging task. *J. Neurosci.* **34**, 646–655 (2014).
23. Wise, S. P. Forward frontal fields: phylogeny and fundamental function. *Trends Neurosci.* **31**, 599–608 (2008).
24. Heilbronner, S. R., Rodriguez-Romaguera, J., Quirk, G. J., Groenewegen, H. J. & Haber, S. N. Circuit-based corticostriatal homologies between rat and primate. *Biol. Psychiatry* **80**, 509–521 (2016).
25. Cole, M. W., Yeung, N., Freiwald, W. A. & Botvinick, M. Cingulate cortex: diverging data from humans and monkeys. *Trends Neurosci.* **32**, 566–574 (2009).
26. Cole, M. W., Yeung, N., Freiwald, W. A. & Botvinick, M. Conflict over cingulate cortex: between-species differences in cingulate may support enhanced cognitive flexibility in humans. *Brain. Behav. Evol.* **75**, 239–240 (2010).
27. Womelsdorf, T. et al. Modulation of neuronal interactions through neuronal synchronization. *Science* **316**, 1609–1612 (2007).
28. Logothetis, N. K., Pauls, J., Augath, M., Trinath, T. & Oeltermann, A. Neurophysiological investigation of the basis of the fMRI signal. *Nature* **412**, 150–157 (2001).
29. Logothetis, N. K. & Wandell, B. A. Interpreting the BOLD signal. *Annu. Rev. Physiol.* **66**, 735–769 (2004).
30. Cavanagh, J. F. & Frank, M. J. Frontal theta as a mechanism for cognitive control. *Trends Cogn. Sci.* **18**, 414–421 (2014).
31. Cavanagh, J. F., Zambrano-Vazquez, L. & Allen, J. J. B. Theta lingua franca: a common mid-frontal substrate for action monitoring processes. *Psychophysiology* **49**, 220–238 (2012).
32. Oehrn, C. R. et al. Neural communication patterns underlying conflict detection, resolution, and adaptation. *J. Neurosci.* **34**, 10438 (2014).
33. Tang, H. et al. Cascade of neural processing orchestrates cognitive control in human frontal cortex. *Elife* **5**, e12352 (2016).
34. Helfrich, R. F. & Knight, R. T. Oscillatory dynamics of prefrontal cognitive control. *Trends Cogn. Sci.* **20**, 916–930 (2016).
35. Pesaran, B. et al. Investigating large-scale brain dynamics using field potential recordings: analysis and interpretation. *Nat. Neurosci.* **21**, 903–919 (2018).
36. Kayser, C., Montemurro, M. A., Logothetis, N. K. & Panzeri, S. Spike-Phase coding boosts and stabilizes information carried by spatial and temporal spike patterns. *Neuron* **61**, 597–608 (2009).
37. Shenhav, A., Botvinick, M. M. & Cohen, J. D. The expected value of control: an integrative theory of anterior cingulate cortex function. *Neuron* **79**, 217–240 (2013).
38. Sheth, S. A. et al. Human dorsal anterior cingulate cortex neurons mediate ongoing behavioural adaptation. *Nature* **488**, 218 (2012).
39. Jensen, O. & Lisman, J. E. Position reconstruction from an ensemble of hippocampal place cells: contribution of theta phase coding. *J. Neurophysiol.* **83**, 2602–2609 (2000).
40. O'Keefe, J. & Burgess, N. Dual phase and rate coding in hippocampal place cells: theoretical significance and relationship to entorhinal grid cells. *Hippocampus* **15**, 853–866 (2005).
41. Montemurro, M. A., Rasch, M. J., Murayama, Y., Logothetis, N. K. & Panzeri, S. Phase-of-Firing coding of natural visual stimuli in primary visual cortex. *Curr. Biol.* **18**, 375–380 (2008).

42. Hawellek, D. J., Wong, Y. T. & Pesaran, B. Temporal coding of reward-guided choice in the posterior parietal cortex. *Proc. Natl Acad. Sci. USA* **113**, 13492–13497 (2016).
43. Constantinescu, A. O., O'Reilly, J. X. & Behrens, T. E. J. Organizing conceptual knowledge in humans with a grid-like code. *Science* **352**, 1464–1468 (2016).
44. O'Keefe, J. & Recce, M. L. Phase relationship between hippocampal place units and the EEG theta rhythm. *Hippocampus* **3**, 317–330 (1993).
45. Cannon, J. et al. Neurosystems: brain rhythms and cognitive processing. *Eur. J. Neurosci.* **39**, 705–719 (2014).
46. Eisenreich, B. R., Akaishi, R. & Hayden, B. Y. Control without controllers: toward a distributed neuroscience of executive control. *J. Cogn. Neurosci.* **29**, 1684–1698 (2017).
47. Ito, T., Tiede, M. & Ostry, D. J. Somatosensory function in speech perception. *Proc. Natl Acad. Sci. USA* **106**, 1245–1248 (2009).
48. Ebitz, R. B. & Platt, M. L. Neuronal activity in primate dorsal anterior cingulate cortex signals task conflict and predicts adjustments in pupil-linked arousal. *Neuron* **85**, 628–640 (2015).
49. Grinvald, A., Kenet, T., Arieli, A. & Tsodyks, M. Are single cortical neurons independent or are they obedient members of a huge orchestra? in *23 Problems in Systems Neuroscience* (eds J. Leo van Hemmen, J. L. & Sejnowski, T. J.) chapter 9 (Oxford Univ. Press, 2006).

Acknowledgements

This work was supported by NIH R01 MH106700 (S.A.S.), NIH K12 NS080223 (S.A.S.), NIH S10 OD018211 (C.A.S.), NIH R01 NS084142 (C.A.S.), NIH R01 DA038615 (B.Y.H.), the Dana Foundation (S.A.S.), the McNair Foundation (S.A.S.), and a Young Investigator grant from the Brain & Behavior Research Foundation (E.H.S). Special thanks to C. Casadei, D. K. Peprah, and T. G. Dyster, all at Columbia University Medical Center, for coordination and data collection efforts.

Author contributions

S.A.S., C.B.M., M.J.Y., and E.H.S. designed the experiments. E.H.S., C.B.M., M.J.Y., Y.J.P., C.A.S., G.M.M., and S.A.S were involved with collecting the data. E.H.S., G.P.B., and G.H. analyzed the data. E.H.S., S.A.S., G.H., B.Y.H., M.M.B., and M.J.Y., wrote the manuscript. All authors provided edits to the manuscript.

Competing interests

The authors declare no competing interests.

Additional information

Supplementary information is available for this paper at https://doi.org/10.1038/s41593-019-0494-0.

Correspondence and requests for materials should be addressed to S.A.S.

Peer review information Nature Neuroscience thanks Tobias Egner and the other, anonymous, reviewer(s) for their contribution to the peer review of this work.

Methods

Participants and ethics statement. Two cohorts of individuals participated in this research. One (Cohort 1, Supplementary Table 2) was a cohort of six patients (one female) with medically refractory epilepsy who were undergoing intracranial monitoring to identify seizure onset regions. These patients had been implanted with stereo-electroencephalography (sEEG) depth electrodes using standard stereotactic techniques. One or more of the sEEG electrodes in this cohort spanned the dlPFC to the dACC (Brodmann's areas 24 a, b, and c, and 32), providing LFP recordings from both regions, as well as single unit recordings in the dACC (see Data acquisition and preprocessing below).

The other cohort (Cohort 2, Supplementary Table 3) was a cohort of nine patients: eight (two female) with movement disorders (Parkinson's disease or essential tremor) who were undergoing DBS surgery, and one male patient with epilepsy undergoing intracranial seizure monitoring. The entry point for the trajectory of the DBS electrode is typically in the inferior portion of the superior frontal gyrus or superior portion of the middle frontal gyrus, within 2 cm of the coronal suture. This area corresponds to the dlPFC (Brodmann's areas 9 and 46). The single epilepsy patient in this cohort underwent a craniotomy for placement of subdural grid and strip electrodes in a prefrontal area including the dlPFC. Thus this cohort provided single-unit and LFP recordings from the dlPFC (see Data acquisition and preprocessing below).

All decisions regarding sEEG and DBS trajectories and craniotomy location were made solely on the basis of clinical criteria. The Columbia University Medical Center Institutional Review Board approved these experiments (IRB-AAAB6324, IRB-AAAB6324, IRB-AAAK2104), and all participants provided informed consent before participating in the study.

Behavioral Task. All participants performed the MSIT (Fig. 1b)[50], in which each trial consisted of a 500 ms fixation period, followed by a cue consisting of three integers ranging from 0 to 3. One of these three numbers (the 'target') was different from the other two numbers (the 'distractors'). Participants were instructed to indicate the identity of the target number on a three-button pad, on which each button represented the integers 1 (left-hand button), 2 (middle button), and 3 (right-hand button). This task therefore presented two types of conflict: spatial conflict if the target was in a different position in the cue than on the three-button pad (that is, '0 0 1'; the target is in the right-hand position, but the left-hand button is the correct choice), and distractor conflict if the distractor numbers were possible button choices (for example '3 2 3', in which 3 corresponds to a possible button choice, versus '0 2 0', in which 0 does not correspond to a possible button choice). After each participant registered his or her response, the cue disappeared and feedback appeared, consisting of the target number in a different color, with a variable delay of 300–800 ms. Valenced feedback (green for correct, red for incorrect) alternated with neutral feedback (blue regardless of correctness) in blocks of ten trials. The inter-trial interval varied uniformly randomly between 1 and 1.5 seconds.

The task was presented on a computer monitor controlled by the Psychophysics Matlab Toolbox (www.psychtoolbox.org, The MathWorks; Matlab v. 2016b-2018b). This software interfaced with data acquisition cards (National Instruments) that allowed for synchronization of behavioral events and neural data with sub-millisecond precision. Differences in log reaction times over conflict conditions were tested using mixed-effects models (LMM):

$$\boldsymbol{y} = \boldsymbol{X}\beta + \boldsymbol{Z}\boldsymbol{u} + \epsilon$$

where y represents reaction times, X represents a design matrix of conflict condition factors, β represents the fixed-effects regression coefficients, Z represents the random-effects design matrix accounting for random variance in participant–session reaction times, u represents the random component of the fixed effects in β, and ϵ represents the model residuals, or, in Wilkinson notation, reaction time ~1 + conflict condition × session + (1 + conflict condition × session | participant). Reaction times were lognormally distributed, so we modeled the log of reaction time to meet assumptions of normality. These models were fit using maximum likelihood methods using the Matlab function fitglme. Subsequent linear models are specified using Wilkinson notation.

Statistics. As described in the previous section, many of the hypotheses were tested with LMMs, the effects of which were evaluated with two-sided t-tests. All statistical tests performed are listed in Supplementary Table 4. For tests that assumed normality, a priori Lilliefors tests were performed to confirm that data were normally distributed. Sample sizes were based on numbers of trials and neurons, both of which were randomized. The number of trials was determined by the patients' willingness and motivation to perform the task. The conflict type for each trial was randomly assigned from a uniform distribution. The number of neurons was based on where microelectrodes ended up recording, approximately 4 mm away from the nearest macroelectrode, which was placed on the basis of clinical parameters. Experimenters were neither able to control the number of trials a patient performed, nor to control the precise location of microelectrodes; nevertheless, we report similar numbers to those reported in previous studies[38,51–53]. Data collection and analysis were not performed blind to the conditions of the experiments.

Data acquisition and preprocessing. Data were acquired at two electrophysiological scales from each participant: SUA and LFPs. SUA was recorded from microelectrodes using three different techniques. In Cohort 1, the dlPFC–dACC sEEG electrodes were Behnke-Fried macro–micro-electrodes (AdTech Medical), which consist of a standard clinical depth macroelectrode shaft with a bundle of eight shielded microwires that protrude approximately 4 mm from the tip. These eight microwires are referenced to a ninth unshielded microwire. dACC SUA was acquired with this technique (Figs. 1b and 2a). Cohort 2 provided dlPFC SUA using two techniques (Fig. 5a). The DBS surgeries were performed according to standard clinical procedure, using clinical microelectrode recording (FHC). Before inserting the guide tubes for the clinical recordings, we placed the microelectrodes in the cortex under direct vision to record from the dlPFC, as we have previously described[52]. The epilepsy implant in Cohort 2 included a UMA implanted in the dlPFC, as we have previously described[54–56]. Data were amplified, high-pass filtered, and digitized at 30 kilosamples per second on a neural signal processor (Blackrock Microsystems) simultaneously with the ECoG data.

LFPs were recorded from subdural ECoG electrodes or standard clinical sEEG macroelectrodes. In Cohort 1, LFP data were recorded from the eight contacts along the clinical ECoG electrode and referenced to either a scalp electrode or a quiescent sEEG contact in the cerebral white matter, depending on the clinical recording configuration. The medial contacts were within the dACC, and lateral contacts within the dlPFC (Fig. 1a). In the DBS patients in Cohort 2, LFP data were recorded from eight-contact (3 mm electrode diameter, 5 mm inter-contact spacing) ECoG strips (PMT). These ECoG strips were slid over the cortical surface through the burr hole adjacent to the microelectrodes and were referenced to scalp needle electrodes adjacent to the mastoid bone. For the epilepsy patient in Cohort 2, LFP data were recorded from the nearest ECoG electrode on the grid overlying the UMA and referenced to an epidural ECoG strip. In all cases, signals from ECoG contacts were pseudodifferentially amplified tenfold and digitized at 2 kHz on the same recording system, and therefore same time base, as the SUA and task event data.

LFP data were preprocessed by first removing clearly broken ECoG or sEEG electrodes and then removing the common mode across channels by reconstructing the data without the first principal component. The resultant time series were then epoched from 2 s before until 3 s after the time of stimulus onset. Trials containing epileptiform discharges were removed based on the range of the LFP voltage across all trials. Trials in which the range of the signal was greater than 1.5 times the interquartile range of the distribution of voltage ranges across all trials were manually reviewed and excluded. LFP spectra between 0 and 150 Hz were calculated with multi-taper methods using the Chronux toolbox for Matlab with five leading tapers and a time-bandwidth product of three.

Action potential sorting. SUA data were re-thresholded offline at −4 × the root mean square of the 250 Hz high-pass filtered signal. Well-isolated action potential waveforms were then segregated in a semi-supervised manner using the T-distribution expectation-maximization method on a feature space comprised of the first three principal components using Offline Sorter software (Plexon)[57]. The times of threshold crossing for identified single units were retained for further analysis.

Classification of single unit selectivity. To estimate neuronal selectivity, we fit a sliding GLM (using similar methods to those used in ref. [10]) to the normalized firing rate of each neuron averaged over a time window of 250 ms each, and repeated this process iteratively, shifting in steps of 20 ms for the duration of the whole trial. This GLM, implemented with custom scripts in Matlab, consisted of a three-way analysis of variance (ANOVA) with factors: decision conflict (four levels: neither conflict, spatial conflict, flanker conflict, and both conflicts), response identity (three levels: button 1, 2, or 3), and feedback valence (two levels: neutral versus valenced feedback). This ANOVA model also accounted for reaction time as a nuisance variable and included interaction terms for all four factors. Using this sliding GLM, we classified individual neurons on the basis of their firing rate selectivity for these task-relevant features.

We focused our analyses on target windows of 500 ms during a post-stimulus period centered 500 ms after stimulus onset rather than on longer time windows so as to limit the number of statistical tests. To establish statistical significance while controlling for multiple tests within each target window (that is, one test for each of 25 20-ms steps), we performed a permutation test in which trains of neuronal spike data corresponding to a trial were randomly reshuffled across trials, for each of the neurons separately, for a total of 10,000 iterations. Using the main three-way ANOVA model with test windows of 250 ms and steps of 20 ms, a combined threshold of $P \leq 0.03$ for at least four consecutive steps yielded significant effects for the first factor (in a 500 ms target window) in less than 5% of the surrogate neurons. The α value of 0.03 was chosen to correct for the number of consecutive bins required to reach significance, and corresponds to a corrected α value of 0.05. This combined significance threshold, which had the higher yet significant P value combined with longer duration, was chosen over a combined threshold of lower P value with shorter duration because meaningful electrophysiological effects (true positives) tend to last for several consecutive timepoints in contrast with noisy effects (false positives). We therefore adopted this combined height-duration threshold in all of our analyses of individual neurons to control for

multiple comparisons. McNemar's test with a Yates' corrected χ^2 were used to test for differences in proportions of neurons. All tests were two-sided.

SFC. SFC was calculated using multi-taper methods with the Chronux toolbox for Matlab[58]. SFC coherograms were generated using a 1 s window size, a 10 ms step size, a time-bandwidth product of five, and nine leading tapers. Significant changes in coherence were determined with permutation tests, for which random trials of SUA and LFP data were paired. Such a randomized trial pairing was performed 10,000 times, and SFC was recalculated between random pairs of SUA and LFP data in order to generate SFC null distributions. Coherograms for each neuron and condition (randomly subsampling numbers of trials such that they were balanced across conditions) were then tested against these null distributions to determine statistically significant frequency bands and time ranges using cluster-corrected permutation tests with significance levels of 0.05 (ref. [59]). Only significant clusters following the onset of the stimulus and before the maximum reaction times were considered. We refer to this procedure as the SFC permutation test. The phase and amplitude of coherence among conditions were then examined for neurons exhibiting significant SFC clusters. To enable comparison with the firing rate models, these phase or reliability coding effects were assessed using a sliding ANOVA over the same time period as that for which firing rate effects were assessed, specifically 250–750 ms following stimulus onset[59].

Single-trial coherence for the UMA data was calculated as described above, except that coherence was calculated across simultaneously recorded neurons for each trial. Ordinary least squares linear regression was used to predict reaction times in each condition from single-trial theta coherence calculated among simultaneously recorded dlPFC neurons. To confirm that the amount of decision conflict on previous trials did not affect our ability to predict reaction time from single trial coherence across a population of dlPFC neurons, we implemented a multiple regression model of reaction time using theta coherence, current trial conflict level, previous trial conflict level, and the interaction between current and previous trial conflict levels as predictors (reaction time ~ 1 + theta coherence + current trial conflict level × previous trial conflict level).

Discriminability. To roughly compare the time courses of conflict effects across coding schemes, we fit a linear discriminant model to each timepoint of the firing rate or coherence phase data across populations of each category of neuron[60]. This model was evaluated with fourfold cross-validation, and a permutation threshold based on reshuffling conflict labels among trial data was used to determine significance (values greater than 95% of the area under the permutation distribution).

stLFPs. To understand the average influence of a dACC neuron's action potential on population synaptic dynamics in the dACC and dlPFC, we aligned 3 s of LFP recorded in the dACC and dlPFC before and after the time of each dACC spike occurring between 250 ms and 750 ms following the stimulus. These LFPs were decorrelated by their covariance matrix and then *z*-scored. Averaging these LFPs generated an stLFP. stLFPs have been shown to be closely related to the cross-correlation of the intracellularly recorded membrane potential and the surrounding LFP[61]. To generate null distributions to test for any stLFP effect, while maintaining both the temporal structure in the population firing rate and each neuron's contribution to the mean population firing rate overall, spikes were also randomly shifted among adjacent 1 ms time bins and across adjacent trials using the raster margins model[62]. Null distributions for stLFP were generated by calculating stLFPs from these shifted spike times and the original LFP as described in the raster margins model. stLFP amplitude was operationally defined as the minimum stLFP during the 200 ms following the mean dACC spike time. Again an LMM was used to assess significance among stLFPs that were associated with particular classes of neurons. The model specification in this case was: stLFP ~ 1 + conflict-selective neurons × session + theta-coherent neurons × session + beta-coherent neurons × session + non-coding neurons × session + (1 + conflict-selective neurons × session + theta-coherent neurons × session + beta-coherent neurons × session + non-coding neurons × session | participant).

Reporting Summary. Further information on research design is available in the Nature Research Reporting Summary linked to this article.

Data availability

Data are available from the authors upon reasonable request and with permission of the Columbia University Medical Center Institutional Review Board.

Code availability

All analysis code is available online at http://www.github.com/elliothsmith/MSIT-analysis

References

50. Bush, G. & Shin, L. M. The multi-source interference task: an fMRI task that reliably activates the cingulo-frontal-parietal cognitive/attention network. *Nat. Protoc.* **1**, 308–313 (2006).
51. Fu, Z. et al. Single-Neuron correlates of error monitoring and post-error adjustments in human medial frontal cortex. *Neuron* **101**, 165–177.e5 (2019).
52. Mian, M. K. et al. Encoding of rules by neurons in the human dorsolateral prefrontal cortex. *Cereb. Cortex* **24**, 807–816 (2014).
53. Jacobs, J. et al. Direct recordings of grid-like neuronal activity in human spatial navigation. *Nat. Neurosci.* **16**, 1188–1190 (2013).
54. Schevon, C. A. et al. Evidence of an inhibitory restraint of seizure activity in humans. *Nat. Commun.* **3**, 1060 (2012).
55. Smith, E. H. et al. The ictal wavefront is the spatiotemporal source of discharges during spontaneous human seizures. *Nat. Commun.* **7**, 11098 (2016).
56. House, P. A., MacDonald, J. D., Tresco, P. A. & Normann, R. A. Acute microelectrode array implantation into human neocortex: preliminary technique and histological considerations. *Neurosurg. Focus* **20**, 1–4 (2006).
57. Shoham, S., Fellows, M. R. & Normann, R. A. Robust, automatic spike sorting using mixtures of multivariate t-distributions. *J. Neurosci. Methods* **127**, 111–122 (2003).
58. Mitra, P. P. & Pesaran, B. Analysis of dynamic brain imaging data. *Biophys. J.* **76**, 691–708 (1999).
59. Maris, E. & Oostenveld, R. Nonparametric statistical testing of EEG- and MEG-data. *J. Neurosci. Methods* **164**, 177–190 (2007).
60. Izenman, A. J. Linear discriminant analysis. *Modern Multivariate Statistical Techniques: Regression, Classification, and Manifold Learning* (ed. Izenman, A. J.) 237–280 (Springer, 2008).
61. Okun, M., Naim, A. & Lampl, I. The subthreshold relation between cortical local field potential and neuronal firing unveiled by intracellular recordings in awake rats. *J. Neurosci.* **30**, 4440–4448 (2010).
62. Okun, M. et al. Diverse coupling of neurons to populations in sensory cortex. *Nature* **521**, 511 (2015).

nature research

Corresponding author(s): Sameer A. Sheth, MD, PhD

Last updated by author(s): 2019-0726

Reporting Summary

Nature Research wishes to improve the reproducibility of the work that we publish. This form provides structure for consistency and transparency in reporting. For further information on Nature Research policies, see Authors & Referees and the Editorial Policy Checklist.

Statistics

For all statistical analyses, confirm that the following items are present in the figure legend, table legend, main text, or Methods section.

n/a	Confirmed	
☐	☒	The exact sample size (*n*) for each experimental group/condition, given as a discrete number and unit of measurement
☐	☒	A statement on whether measurements were taken from distinct samples or whether the same sample was measured repeatedly
☐	☒	The statistical test(s) used AND whether they are one- or two-sided *Only common tests should be described solely by name; describe more complex techniques in the Methods section.*
☐	☒	A description of all covariates tested
☐	☒	A description of any assumptions or corrections, such as tests of normality and adjustment for multiple comparisons
☐	☒	A full description of the statistical parameters including central tendency (e.g. means) or other basic estimates (e.g. regression coefficient) AND variation (e.g. standard deviation) or associated estimates of uncertainty (e.g. confidence intervals)
☐	☒	For null hypothesis testing, the test statistic (e.g. *F*, *t*, *r*) with confidence intervals, effect sizes, degrees of freedom and *P* value noted *Give P values as exact values whenever suitable.*
☐	☒	For Bayesian analysis, information on the choice of priors and Markov chain Monte Carlo settings
☐	☒	For hierarchical and complex designs, identification of the appropriate level for tests and full reporting of outcomes
☐	☒	Estimates of effect sizes (e.g. Cohen's *d*, Pearson's *r*), indicating how they were calculated

Our web collection on statistics for biologists contains articles on many of the points above.

Software and code

Policy information about availability of computer code

Data collection	Neural data collection utilized Blackrock Microsystems Central Software (version). Behavioral data collection utilized Psychophysics Toolbox (version 3)
Data analysis	Data analyses were carried out using the chronux toolbox (version 2), Plexon Offline Sorter (version 3.4), and custom Matlab scripts uploaded to github.com/elliothsmith/MSIT-analysis

For manuscripts utilizing custom algorithms or software that are central to the research but not yet described in published literature, software must be made available to editors/reviewers. We strongly encourage code deposition in a community repository (e.g. GitHub). See the Nature Research guidelines for submitting code & software for further information.

Data

Policy information about availability of data

All manuscripts must include a data availability statement. This statement should provide the following information, where applicable:

- Accession codes, unique identifiers, or web links for publicly available datasets
- A list of figures that have associated raw data
- A description of any restrictions on data availability

Data are available from the authors upon reasonable request and with permission of the Columbia University Medical Center Institutional Review Board.

Field-specific reporting

Please select the one below that is the best fit for your research. If you are not sure, read the appropriate sections before making your selection.

☒ Life sciences ☐ Behavioural & social sciences ☐ Ecological, evolutionary & environmental sciences

Life sciences study design

All studies must disclose on these points even when the disclosure is negative.

Sample size	Sample sizes were based on numbers of trials and neurons, both of which were randomized. The number of trials was determined by the patients' willingness and motivation to perform the task. The conflict type for each trial was randomly assigned from a uniform distribution. The number of neurons was based on where microelectrodes ended up recording, approximately 4 mm away from the nearest macroelectrode, which was placed based on clinical parameters. Experimenters were neither able to control the number of trials a patient performed, nor the precise location of microelectrodes.
Data exclusions	Trials containing epileptiform discharges were removed based on the range of the LFP voltage across all trials. Those trials in which the range of the signal was greater than 1.5 times the interquartile range of the distribution of voltage ranges across all trials were manually reviewed and excluded.
Replication	Cross validation and statistical controls were used when possible. Replication for this study mainly involved determining that neuron-level effects were present across subjects.
Randomization	Randomization was carried out by the task, which was determined by a randomly seeded random number generator in Matlab.
Blinding	Subject-level blinding was not possible at the time of data acquisition, though researchers were blinded to trial-level, and neuron-level information at the time of acquisition.

Reporting for specific materials, systems and methods

We require information from authors about some types of materials, experimental systems and methods used in many studies. Here, indicate whether each material, system or method listed is relevant to your study. If you are not sure if a list item applies to your research, read the appropriate section before selecting a response.

Materials & experimental systems

n/a	Involved in the study
☒	☐ Antibodies
☒	☐ Eukaryotic cell lines
☒	☐ Palaeontology
☒	☐ Animals and other organisms
☐	☒ Human research participants
☒	☐ Clinical data

Methods

n/a	Involved in the study
☒	☐ ChIP-seq
☒	☐ Flow cytometry
☒	☐ MRI-based neuroimaging

Human research participants

Policy information about studies involving human research participants

Population characteristics	Subjects were neurosurgical patients undergoing monitoring for medically refractory epilepsy or surgical implantation of deep brain stimulation electrodes. Subjects ranged in age from N to N years. N out of N subjects were female.
Recruitment	All patients who were undergoing the aforementioned surgeries were asked if they would like to participate in the research. No patients declined to participate, suggesting a lack of self-selection bias. The only potential selection bias results form these patients neurological disorders.
Ethics oversight	the Columbia University Medical Center Institutional Review Board approved these experiments.

Note that full information on the approval of the study protocol must also be provided in the manuscript.